ChemComm

CrossMark
click for updates

Halogen bonding between metal centers and halocarbons†

Daniil M. Ivanov,[a] Alexander S. Novikov,[a] Ivan V. Ananyev,[b] Yulia V. Kirina[a] and Vadim Yu. Kukushkin*[a]

Metal-involving halogen bonding was detected in a series of associates of CHI_3 with *trans*-[$PtX_2(NCNAlk_2)_2$] (X = Cl, Br). The $HI_2C–I \cdots \eta^1_{(Pt)}$ halogen bonding and the bifurcated $HI_2C–I \cdots \eta^2_{(Pt–Cl)}$ halogen bonding – the latter undergoes the thermally induced reversible $HI_2C–I \cdots \eta^2_{(Pt–Cl)} \rightleftarrows HI_2C–I \cdots \eta^1_{(Pt)}$ transformation – were observed and confirmed theoretically.

Halogen bonding (XB), among various non-covalent weak inter-actions, is one of the most intensively studied systems in modern science. Together with hydrogen bonding, π–π-, and metallophilic interactions, it is successfully applied in crystal engineering[1,2] and design of compounds exhibiting pharmaco-logical significance.[3–5] Recent applications of XB include stabilization of explosives[6] and molecular design of materials with tunable photophysical properties.[7,8]

In accord with the IUPAC definition, XB[9] is the real R–X$\cdots$Y (X = halogen) contact, when, firstly, the interatomic distance between X and an appropriate nucleophilic atom of Y (Y = F, O, N, Cl, *etc.*) is less than the sum of their van der Waals radii and, secondly, the $\angle$(R–X$\cdots$Y) angle is close to 180° (exceptions from the linearity have been reviewed[10]). These geometrical parameters are usually easily obtained using single-crystal X-ray diffraction (XRD), which is the most common method for the detection of XB. When application of the two criteria in XRD data fails, some other criteria (lengthening of R–X covalent bonds due to XB and also changes in the appropriate spectroscopic parameters[9]), or

application of some other indirect methods, *e.g.* UV-vis, IR and Raman spectroscopy,[11,12] differential anomalous X-ray scattering studies,[13] NMR,[14,15] and phosphorescence[7] spectroscopy, were also applied for XB recognition.

In the majority of the reported cases when XB was reliably identified, only typical Lewis basic non-metal atoms bearing lone pairs (*viz.* O, N, S, halogens *etc.*) behave as XB acceptors, whereas possible XBs with metal centers was found only for I_2.[16–19] Our inspection of the relevant literature indicates few experimental studies describing X$\cdots$M short contacts, which were either not considered as halogen bonds, or their geometrical parameters fulfill only one of the two aforementioned structural IUPAC criteria. Therefore definitive attribution of these weak interac-tions to XB was not provided and the other IUPAC criteria should be applied for their identification. Indeed, Chen *et al.*,[20] Wölper *et al.*,[21] and Laguna *et al.*[22] observed X$\cdots$Au^I and X$\cdots$Ag^I contacts, which fulfilled only the "van der Waals criterion", but in all the three cases the corresponding R–X$\cdots$M angles strongly deviate from 180° (by 30–90°,[20] 60–70°,[21] and 85°[22]) thus contrasting with the second structural IUPAC criterion. Yamamoto *et al.*[23] and Liau *et al.*[24] reported, respectively, the I$\cdots$Au^I and Cl$\cdots$Au^I contacts, which can be interpreted as X$\cdots$Au^I halogen bonds, but the nature of these contacts was not verified. Finally, Blakey *et al.*[25] observed contacts between the typical XB donors such as iodoperfluorobenzenes and gold nanoparticles in water solutions, but these halogen bonds were confirmed only by indirect methods such as UV-vis difference spectroscopy, SERS, and XPS and the geometrical parameters were not obtained.

It is important that a metal atom can be an XB acceptor if it contains at least one lone pair, which could interact with empty σ*-orbitals of an XB donor. In particular, some d^8-Pt^{II} and d^8-Rh^I centers may behave similarly to d^{10}-Au^I ones as these centers feature lone pairs on $4d_{z^2}$ or $5d_{z^2}$ orbitals. In particular, weak contacts were observed between some d^8-Pt^{II} and d^8-Rh^I species and iodine.[16–19] These two were the only reports on unambiguous recognition of metal-involving XB.

Taking into account that no data for XB between metal centers and halocarbons were published, we focused our efforts

[a] *Institute of Chemistry, Saint Petersburg State University, Universitetskaya Nab., 7/9, 199034, Saint Petersburg, Russian Federation. E-mail: v.kukushkin@spbu.ru*

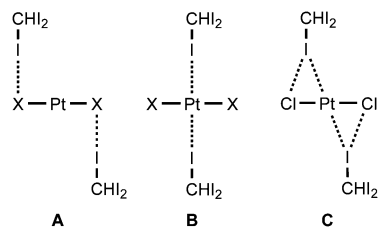[b] *A. N. Nesmeyanov Institute of Organoelement Compounds, Russian Academy of Sciences, Vavilova St., 28, 119991, Moscow, Russian Federation*

Chart 1 Three types of XB between the linear PtX$_2$ (X = Cl, Br) fragment and two CHI$_3$ molecules.

on the search of metal-involving XB and we applied platinum(II) species as potential XB donors and iodoform as an XB acceptor.

In the current work, we report that the dialkylcyanamide d^8-Pt^{II} complexes *trans*-[PtX$_2$(NCNR$_2$)$_2$] (R$_2$ = Me$_2$, X = Cl **1a**, Br **1b**; Et$_2$ **2**, (CH$_2$)$_4$ **3**, (CH$_2$)$_5$ **4**) easily co-crystallize with iodoform taken as the XB donor. We observed that CHI$_3$ tends to co-crystallize with **1a–b** and **4** forming HI$_2$C–I⋯Pt metal-involving halogen bonds (Chart 1, **B**) that fulfill both structural IUPAC criteria for halogen bonding. The existence of metal-involving halogen bonding has also been confirmed theoretically by the combination of DFT and AIM[26] methods. Within the AIM theory, the (3, −1) critical points (bond critical points, BCPs) on the surface of the theoretical electron density function $\rho(r)$ unambiguously reveal all bonding intermolecular interactions, including non-covalent interactions. Energies for the corresponding contacts E_{int} can be determined using semi-empirical correlations between local energy densities in BCPs and interaction strength.[27,28] Moreover, we found and confirmed theoretically by combination of DFT and AIM methods the unique bifurcated HI$_2$C–I⋯$\eta^2_{(Pt–Cl)}$ (**C**) XB that undergoes thermally induced reversible HI$_2$C–I⋯$\eta^2_{(Pt–Cl)} \rightleftarrows$ HI$_2$C–I⋯$\eta^1_{(Pt)}$ transformation.

Complexes **1a** and **1b** form isostructural associates **1a**·½CHCl$_3$· 1½CHI$_3$, **1a**·2CHI$_3$, and **1b**·2CHI$_3$ upon crystallization from **1a**: CHI$_3$ = 1:2 (molar ratio) solutions in chloroform or dichloromethane, or from **1b**:CHI$_3$ = 1:2 (molar ratio) solution in dichloromethane, respectively. Apart from numerous HI$_2$C–I⋯X–Pt halogen bonds (Chart 1, **A**), they exhibit the HI$_2$C–I⋯Pt short contacts, which can be interpreted as metal-involving XB accordingly to both structural IUPAC criteria as the distances I⋯Pt (3.4276(5) Å, 3.4389(5) Å, and 3.4023(5) Å) are less than sums of Bondi's[29] vdW radii (R_{vdW}(Pt) + R_{vdW}(I) = 3.73 Å) and the corresponding angles (164.84(17)°, 169.8(3)°, and 172.7(2)°) are close to 180° (for more details see Section XR2 of the ESI†). We also confirmed the formation of the I⋯Pt non-covalent interaction in **1a**·½CHCl$_3$·1½CHI$_3$ and **1b**·2CHI$_3$ systems theoretically for the **1a**·(CHI$_3$)$_6$ and **1b**·(CHI$_3$)$_6$ model structures by using Bader's AIM analysis (Fig. 1 and 2; for details see Section TH1 in the ESI†). The estimated energies (E_{int}) of these contacts are in the ranges of 2.4–2.8 kcal mol^{-1} and 2.7–3.1 kcal mol^{-1}, respectively. The strength of these weak interactions has been defined according to the procedures proposed by Espinosa *et al.*[27] and Vener *et al.*,[28] these approaches considered explore linear relationships between the local electronic potential $V(r)$ and kinetic $G(r)$ densities at the bond critical points and energies of appropriate contacts.
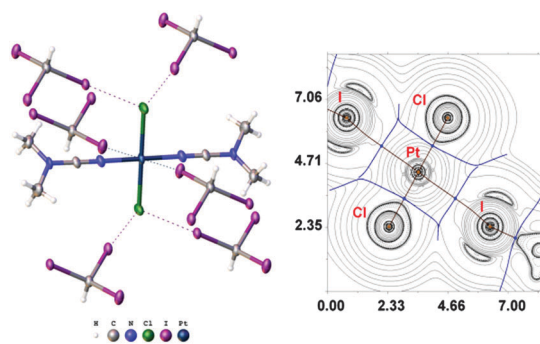

Fig. 1 Left: View of fragment **1a**·(CHI$_3$)$_6$ from **1a**·½CHCl$_3$·1½CHI$_3$. Thermal ellipsoids are shown with 50% probability and short contacts are indicated by dotted lines. Coordinates of this fragment were applied in further DFT calculations. Right: Contour line diagram of the Laplacian distribution $\nabla^2\rho(r)$ (cross-section along the plane Pt–Cl–I) was received as a result of the topological analysis of the electron density distribution in the model structure. Bond paths are shown as brown lines, selected zero-flux surfaces − as blue lines, bond critical points (3, −1) are shown in blue, nuclear critical points (3, −3) − in pale brown, length unit − Å.
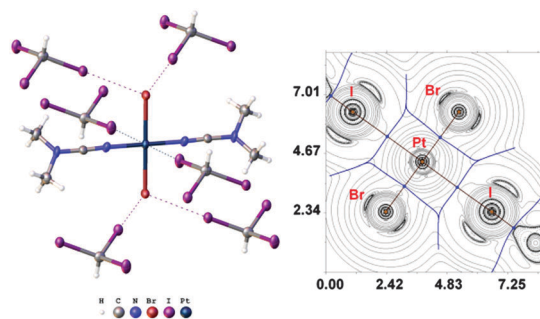

Fig. 2 Left: View of fragment **1b**·(CHI$_3$)$_6$ from **1b**·2CHI$_3$. Thermal ellipsoids are shown with 50% probability and short contacts are indicated by dotted lines. Coordinates of this fragment were applied in further DFT calculations. Right: Contour line diagram of the Laplacian distribution $\nabla^2\rho(r)$ (cross-section along the plane Pt–Br–I) was received as a result of the topological analysis of the electron density distribution in the model structure. Bond paths are shown as brown lines, selected zero-flux surfaces − as blue lines, bond critical points (3, −1) are shown in blue, nuclear critical points (3, −3) − in pale brown, length unit − Å.

Complex **4** was co-crystallized with CHI$_3$ in a 1:2 molar ratio from chloroform solution forming **4**·2CHI$_3$. Apart from two types of HI$_2$C–I⋯Cl–Pt XB (Chart 1, **A**), this solid also contains the bifurcated HI$_2$C–I⋯$\eta^2_{(Pt–Cl)}$ metal-involving XB (**C**). Both distances (d(I⋯Pt) = 3.7060(7) Å and d(I⋯Cl) = 3.6974(19) Å) are slightly less than the corresponding sums of Bondi's[29] vdW radii (R_{vdW}(Pt) + R_{vdW}(I) = 3.73 Å; R_{vdW}(Cl) + R_{vdW}(I) = 3.73 Å) and both contact angles are not much different from 160° (∠(C–I⋯Pt) = 158.4(2)°, ∠(C–I⋯Cl) = 163.4(2)°) (see Section XR2 of the ESI†). The formation of the I⋯Pt and I⋯Cl non-covalent interactions was confirmed theoretically for the **4**·(CHI$_3$)$_6$ model structure by using Bader's AIM analysis (Fig. 3, see also TH1 of the ESI†). The estimated energies E_{int} of these contacts are in good agreement with the energy range for XB (1.3–1.4 kcal mol^{-1} for HI$_2$C–I⋯Cl and 1.6 kcal mol^{-1} for HI$_2$C–I⋯Pt). To the best of our knowledge, these weak
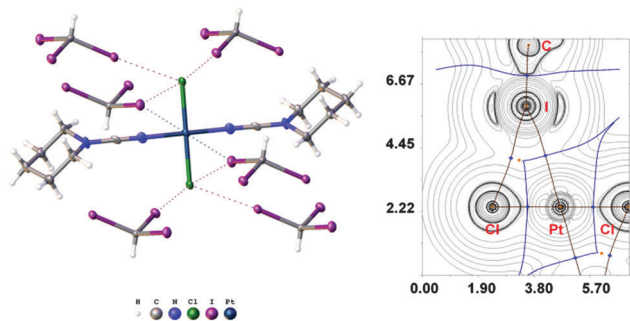
Fig. 3 Left: View of fragment **4**·(CHI$_3$)$_6$ from **4**·2CHI$_3$. Thermal ellipsoids are shown with 50% probability and short contacts are indicated by dotted lines. Coordinates of this fragment were applied in further DFT calculations. Right: Contour line diagram of the Laplacian distribution $\nabla^2\rho(r)$ (cross-section along the plane Pt–Cl–I) was received as a result of the topological analysis of the electron density distribution in the model structure. Bond paths are shown as brown lines, selected zero-flux surfaces – as blue lines, bond critical points (3, −1) are shown in blue, ring critical points (3, +1) – in orange, nuclear critical points (3, −3) – in pale brown, length unit – Å.
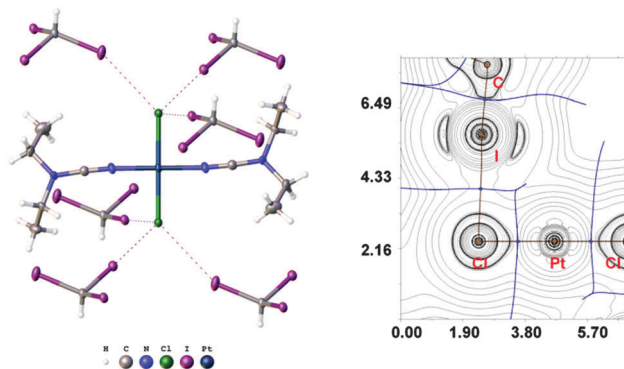

Fig. 4 Left: View of fragment **2**·(CHI$_3$)$_6$ from **2**·2CHI$_3$. Thermal ellipsoids are shown with 50% probability and short contacts are indicated by dotted lines. Coordinates of this fragment were applied in further DFT calculations. Right: Contour line diagram of the Laplacian distribution $\nabla^2\rho(r)$ (cross-section along the plane Pt–Cl–I) was received as a result of the topological analysis of the electron density distribution in the model structure. Bond paths are shown as brown lines, selected zero-flux surfaces – as blue lines, bond critical points (3, −1) are shown in blue, nuclear critical points (3, −3) – in pale brown, length unit – Å.

interactions are the first example of metal-involving bifurcated XB. It is noteworthy that examples of metal-free bifurcated XB[6] and metal-involving bifurcated hydrogen bonding[30] are known. Taking into account that the observed distances within the HI$_2$C–I$\cdots\eta^2_{(Pt–Cl)}$ moiety are only slightly less than their van der Waals separations, more examples of metal-involving bifurcates are needed to exclude completely the packing effects on the bonding.

Variable temperature XRD experiments for the same single-crystal of **4**·2CHI$_3$ were performed at 100, 150, 200, 250, and 300 K. An inspection of the obtained data indicates that the heating leads only to the elongation of the intermolecular distances, whereas the covalent bond lengths remain almost the same. The most significant changes were detected for the bifurcated HI$_2$C–I$\cdots\eta^2_{(Pt–Cl)}$ contacts (by 0.08 Å upon an increase in temperature from 100 to 300 K), whereas the HI$_2$C–I$\cdots$Cl–Pt halogen bonds were lengthened by only 0.05 and 0.03 Å, correspondingly (see also XR3 of the ESI†). Bader's AIM analysis (TH2 of ESI†) for the **4**·(CHI$_3$)$_6$ model systems at each temperature indicated above showed the gradual reduction of the estimated energies of all halogen bonds. Apart from that one of the bond critical points (between Cl and I) in the bifurcated XB disappeared on going from 250 to 300 K. The reversibility of the thermal transformation was proved by three consecutive XRD experiments for the same single-crystal at 100 K, 300 K, and again at 100 K. This experiment gives evidence supporting the thermally induced reversible HI$_2$C–I$\cdots\eta^2_{(Pt–Cl)} \rightleftarrows$ HI$_2$C–I$\cdots\eta^1_{(Pt)}$ transformation.

Complexes **2** and **3** were co-crystallized with CHI$_3$ in a 1 : 2 molar ratio from chloroform solutions forming **2**·2CHI$_3$ and **3**·2CHI$_3$, respectively. These associates were found to form only three types of HI$_2$C–I$\cdots$Cl–Pt XB in each case (Fig. 4 and 5). In all cases (**1a**·$\frac{1}{2}$CHCl$_3$·1$\frac{1}{2}$CHI$_3$, **1b**·2CHI$_3$, **2**·2CHI$_3$, **3**·2CHI$_3$, and **4**·2CHI$_3$), the formation of halogen bonds with the halide ligands was confirmed theoretically by using Bader's AIM
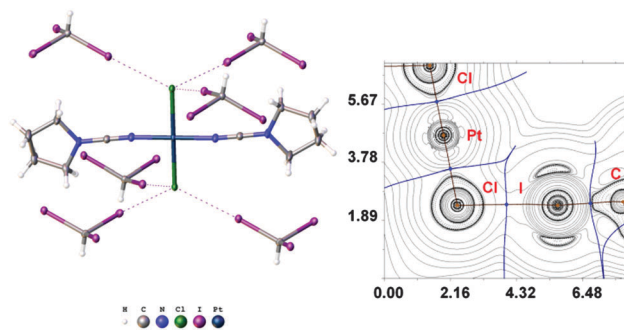

Fig. 5 Left: View of fragment **3**·(CHI$_3$)$_6$ from **3**·2CHI$_3$. Thermal ellipsoids are shown with 50% probability and short contacts are indicated by dotted lines. Coordinates of this fragment were applied in further DFT calculations. Right: Contour line diagram of the Laplacian distribution $\nabla^2\rho(r)$ (cross-section along the plane Pt–Cl–I) was received as a result of the topological analysis of the electron density distribution in the model structure. Bond paths are shown as brown lines, selected zero-flux surfaces – as blue lines, bond critical points (3, −1) are shown in blue, nuclear critical points (3, −3) – in pale brown, length unit – Å.

analysis (XR2 and TH1 of the ESI†). The estimated energies (E_{int}) of this type of weak interaction are in the range of 1.9–3.5 kcal mol^{-1}. Only the HI$_2$C–I$\cdots$Cl$^-$ and the HI$_2$C–I$\cdots$Br$^-$ weak interactions were previously described,[31] but no single example of the XB between metal-coordinated chloride or bromide and CHI$_3$ has been previously reported.

The elongation of the Pt–X (X = Cl, Br) bonds in the CHI$_3$-associates was detected when XRD data of the associates were compared with those of CHI$_3$-free **1a**,[32] **1b**, and **4**[33] (see XR1 in the ESI†). The Pt–Cl distances in **2**·2CHI$_3$ and **3**·2CHI$_3$ are longer than in CHI$_3$-free complexes **1a** and **4**. Although these differences are not too large (0.01–0.03 Å), the observed elongation indirectly point out (Chart 2) to the presence of the HI$_2$C–I$\cdots$X–Pt and HI$_2$C–I$\cdots$Pt contacts (see XR2 and TH1 in the ESI†) additionally supporting our conclusions.
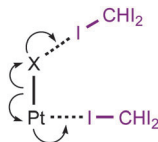
Chart 2 The Pt–X bond elongation caused by the HI$_2$C–I···X–Pt and HI$_2$C–I···Pt weak interactions.

In this communication, we reported the first examples of definite and unambiguous identification of metal-involving XB with halocarbons, *viz.* between Pt^{II} and CHI$_3$. Various Pt^{II} centers are known to participate in donor–acceptor interactions with Lewis acids (B^{III} and S^{IV} compounds[34,35]), but in all cases these donor–acceptor bonds are too strong to be treated as non-covalent bonds. The most relevant example of XB is weak contacts between the Pt^{II} and Rh^{I} centers and iodine.[16–19] Examples of the X···M short contacts given in the Introduction have not been clearly identified as metal-involving XB. We plan to continue our studies in the area of metal-involving XB and to expand the range of studied systems to other X's and X-containing species (*e.g.* Br) and metal centers (*e.g.* Pd^{II}) and studies in these directions are underway in our group.

References

1 R. Bertani, P. Sgarbossa, A. Venzo, F. Lelj, M. Amati, G. Resnati, T. Pilati, P. Metrangolo and G. Terraneo, *Coord. Chem. Rev.*, 2010, **254**, 677–695.
2 G. Cavallo, P. Metrangolo, T. Pilati, G. Resnati, M. Sansotera and G. Terraneo, *Chem. Soc. Rev.*, 2010, **39**, 3772–3783.
3 E. Persch, O. Dumele and F. Diederich, *Angew. Chem., Int. Ed.*, 2015, **54**, 3290–3327.
4 P. Auffinger, F. A. Hays, E. Westhof and P. S. Ho, *Proc. Natl. Acad. Sci. U. S. A.*, 2004, **101**, 16789–16794.
5 P. S. Ho, *Halogen Bonding I: Impact on Materials Chemistry and Life Sciences*, Springer-Verlag Berlin, Berlin, 2015, vol. 358, pp. 241–276.
6 K. B. Landenberger, O. Bolton and A. J. Matzger, *J. Am. Chem. Soc.*, 2015, **137**, 5074–5079.
7 H. Wang, R. X. Hu, X. Pang, H. Y. Gao and W. J. Jin, *CrystEngComm*, 2014, **16**, 7942–7948.
8 V. V. Sivchik, A. I. Solomatina, Y.-T. Chen, A. J. Karttunen, S. P. Tunik, P.-T. Chou and I. O. Koshevoy, *Angew. Chem., Int. Ed.*, 2015, **54**, 14057–14060.
9 G. R. Desiraju, P. S. Ho, L. Kloo, A. C. Legon, R. Marquardt, P. Metrangolo, P. Politzer, G. Resnati and K. Rissanen, *Pure Appl. Chem.*, 2013, **85**, 1711–1713.
10 K. Rissanen, *CrystEngComm*, 2008, **10**, 1107–1113.
11 S. V. Rosokha, C. L. Stern and J. T. Ritzert, *Chem. – Eur. J.*, 2013, **19**, 8774–8788.
12 D. A. Bahnick, W. E. Bennett and W. B. Person, *J. Phys. Chem.*, 1969, **73**, 2309–2316.
13 T. Mager, H. Bertagnolli, D. Degenhardt and R. Frahm, *Mol. Phys.*, 1991, **73**, 587–601.
14 H. G. Lohr, A. Engel, H. P. Josel, F. Vogtle, W. Schuh and H. Puff, *J. Org. Chem.*, 1984, **49**, 1621–1627.
15 J. Viger-Gravel, S. Leclerc, I. Korobkov and D. L. Bryce, *J. Am. Chem. Soc.*, 2014, **136**, 6929–6942.
16 J. A. M. van Beek, G. van Koten, G. Dekker, E. Wissing, M. C. Zoutberg and C. H. Stam, *J. Organomet. Chem.*, 1990, **394**, 659–678.
17 J. A. M. van Beek, G. van Koten, W. J. J. Smeets and A. L. Spek, *J. Am. Chem. Soc.*, 1986, **108**, 5010–5011.
18 R. A. Gossage, A. D. Ryabov, A. L. Spek, D. J. Stufkens, J. A. M. van Beek, R. van Eldik and G. van Koten, *J. Am. Chem. Soc.*, 1999, **121**, 2488–2497.
19 D. W. Shaffer, S. A. Ryken, R. A. Zarkesh and A. F. Heyduk, *Inorg. Chem.*, 2012, **51**, 12122–12131.
20 J. H. Chen, Y. M. Liu, J. X. Zhang, Y. Y. Zhu, M. S. Tang, S. W. Ng and G. Yang, *CrystEngComm*, 2014, **16**, 4987–4998.
21 C. Wölper, S. R. Piñol, S. D. Ibáñez, M. Freytag, P. G. Jones and A. Blaschette, *Z. Anorg. Allg. Chem.*, 2008, **634**, 1506–1516.
22 A. Laguna, T. Lasanta, J. M. Lopez-de-Luzuriaga, M. Monge, P. Naumov and M. E. Olmos, *J. Am. Chem. Soc.*, 2010, **132**, 456–457.
23 H. M. Yamamoto, J. I. Yamaura and R. Kato, *J. Am. Chem. Soc.*, 1998, **120**, 5905–5913.
24 R. Y. Liau, H. Ehlich, A. Schier and H. Schmidbaur, *Z. Naturforsch., B: J. Chem. Sci.*, 2002, **57**, 1085–1089.
25 I. Blakey, Z. Merican, L. Rintoul, Y. M. Chuang, K. S. Jack and A. S. Micallef, *Phys. Chem. Chem. Phys.*, 2012, **14**, 3604–3611.
26 R. F. W. Bader, *Atoms in Molecules: A Quantum Theory*, Oxford University Press, Oxford, 1990.
27 E. Espinosa, E. Molins and C. Lecomte, *Chem. Phys. Lett.*, 1998, **285**, 170–173.
28 M. V. Vener, A. N. Egorova, A. V. Churakov and V. G. Tsirelson, *J. Comput. Chem.*, 2012, **33**, 2303–2309.
29 A. Bondi, *J. Phys. Chem.*, 1964, **68**, 441–451.
30 D. Braga, F. Grepioni, E. Tedesco, K. Biradha and G. R. Desiraju, *Organometallics*, 1997, **16**, 1846–1856.
31 H. Bock and S. Holl, *Z. Naturforsch., B: J. Chem. Sci.*, 2001, **56**, 152–163.
32 N. A. Bokach, T. B. Pakhomova, V. Y. Kukushkin, M. Haukka and A. J. L. Pombeiro, *Inorg. Chem.*, 2003, **42**, 7560–7568.
33 P. V. Gushchin, N. A. Bokach, M. Haukka, E. S. Dmitrieva and V. Y. Kukushkin, *Acta Crystallogr., Sect. E: Struct. Rep. Online*, 2006, **62**, m244–m246.
34 S. Bontemps, M. Sircoglou, G. Bouhadir, H. Puschmann, J. A. K. Howard, P. W. Dyer, K. Miqueu and D. Bourissou, *Chem. – Eur. J.*, 2008, **14**, 731–740.
35 P. Steenwinkel, H. Kooijman, W. J. J. Smeets, A. L. Spek, D. M. Grove and G. van Koten, *Organometallics*, 1998, **17**, 5411–5426.